Effect of Sphingomyelin Composition on the Phase Structure of Phosphatidylcholine−Sphingomyelin Bilayers†

Liliana K. Bar,‡,§,|| Yechezkel Barenholz,*,§ and Thomas E. Thompson‡

Department of Biochemistry, University of Virginia, Charlottesville, Virginia 22908, and Department of Biochemistry, The Hebrew University of Jerusalem, P.O. Box 12272, Jerusalem 91120, Israel

Received October 7, 1996; Revised Manuscript Received December 18, 1996⊗

ABSTRACT: In this study, we examine the phase behavior as well as lateral diffusion and percolation in the region of coexisting gel and fluid phases in binary mixtures composed of dimyristoylphosphatidylcholine and one of two totally synthetic D-*erythro*-sphingomyelins (having either C16 or C24 acyl chains, both having similar gel to liquid-crystalline phase transition temperatures). This study stems from the uniqueness of sphingomyelins having gel to liquid-crystalline transition temperatures in the range of physiological interest, and the fact that more than 50% of the naturally occurring sphingomyelin species have a chain mismatch. The presence of sphingomyelin in biological membranes can thus be expected to give rise to a complex phase structure. Fluorescence recovery after photobleaching, differential scanning calorimetry, and electron microscopy are used to show that, despite similarity in the temperature range of the gel to liquid-cystalline phase transition of the two sphingomyelins, the two differ in their phase structure. Also they differ to a large extent in their mixing with dimyristoylphosphatidylcholine. Dimyristoylphosphatidylcholine and C16 sphingomyelin mix nearly ideally, with the percolation threshold locus lying close to the liquidus on the phase diagram. In contrast, the C24 sphingomyelin and dimyristoylphosphatidylcholine mix nonideally, with the percolation threshold locus lying close to the solidus. In addition, mixtures containing C24 sphingomyelin have a complex thermotropic behavior which may be related to the observation that these dispersions contain several types of particles, some of which are not multilamellar vesicles. These studies suggest that the degree of sphingomyelin chain mismatch is an important factor in determining lateral organization in the membrane.

There is considerable evidence, both direct and indirect, that a microdomain structure exists in the plasma membranes of a number of different cell types (Jacobson & Vaz, 1992; Bergelson et al., 1995). This view, in addition to the fact that membranes are multicomponent systems with their two faces compositionally distinct, constitutes an important modification of the now classical Singer−Nicholson model (1972) of biological membrane structure. Although there is no agreement about the molecular basis of this domain structure, it is possible that the phase structure of the lipid bilayer component of biological membranes may be responsible for it, at least in part. For this to be the case, biomembranes from mammalian cells must contain in their bilayers substantial amounts of lipids with transition temperatures in the region of 37 °C. Sphingomyelins are good candidates as molecules which have the potential to introduce lateral heterogeneity and immiscibility in the membrane plane, as all naturally occurring sphingomyelins have phase transitions in the range of 30−45 °C (Barenholz & Thompson, 1980; Barenholz & Gatt, 1982; Barenholz, 1984). The role of sphingomyelin in generating a phase domain structure in biomembranes is supported by studies in rat cardiomyocytes in culture (Yechiel et al., 1985).

All natural sphingomyelins have the D-*erythro*-(*2S*,3*R*) configuration in the sphingosine moiety. The latter contributes one hydrophobic chain to the molecule, having an effective length in the hydrophobic core of the bilayer of 13.5 carbons (Huang & Mason, 1986). The second methylene chain is contributed by an acyl residue in amide linkage to sphingosine. It is usually fully saturated or monounsaturated. Typically, more than 50% of sphingomyelin species of mammalian tissues (except red blood cells) have a chain mismatch, as their acyl chain is longer than 20 carbons (Barenholz, 1984).

In this study, binary mixtures of two totally synthetic D-*erythro*-sphingomyelins (either C16-SPM or C24-SPM)[1] with dimyristoylphosphatidylcholine have been examined by fluorescence recovery after photobleaching (FRAP) to characterize lateral diffusion and percolation properties of the coexisting phases (Vaz et al., 1989). The synthetic *N*-palmitoyl-SPM (C16-SPM) is a molecule having its acyl chain of nearly equal length to its sphingosine methylene chain. The other sphingomyelin, with a lignoceryl (C24) acyl chain, gives a large length mismatch between the very long acyl chain and the much shorter sphingosine methylene chain. In addition to the FRAP studies, dispersions of the

† This work was supported by NIH Grants GM-14628, GM-23573 (to T.E.T.), and HL-17576 (to Y.B.) and by United States−Israel Binational Science Foundation Grant 95/318 (to T.E.T. and Y.B.).

* To whom correspondence should be addressed.
‡ University of Virginia.
§ The Hebrew University of Jerusalem.
|| Present address: Omrix, Rehovot, Israel.

⊗ Abstract published in *Advance ACS Abstracts,* February 1, 1997.

[1] Abbreviations: SPM, sphingomyelin; C16-SPM, D-*erythro*-2-*N*-palmitoylsphingosyl-1-phosphocholine; C24-SPM, D-*erythro*-2-*N*-lignocerylsphingosyl-1-phosphocholine; DMPC, 1,2-dimyristoyl-*sn*-glycero-3-phosphocholine; DLPE-NBD, *N*-(7-nitro-2-1,3-benzoxadiazol-4-yl)-1,2-dilauroylphosphatidylethanolamine; DSC, differential scanning calorimetry; FRAP, fluorescence recovery after photobleaching; MLV, multilamellar vesicles; PC, phosphatidylcholine; QUELS, quasi-elastic light scattering.

S0006-2960(96)02500-7 CCC: $14.00 © 1997 American Chemical Society

pure phospholipid components as well as the binary mixtures have been examined by differential scanning calorimetry (DSC) in order to construct rough phase diagrams. Selected aqueous dispersions of the pure components and the mixtures have also been examined by freeze−etch electron microscopy.

MATERIALS AND METHODS

D-*erythro*-2-*N*-Palmitoylsphingosyl-1-phosphocholine (C16-SPM) and D-*erythro*-2-*N*-lignocerylsphingosyl-1-phosphocholine (C24-SPM) were purchased from Lipitek (San Antonio, TX). Both sphingomyelins were further purified by four precipitations with cold acetone from chloroform/methanol (10:1, v/v). The purity of the sphingomyelins was assessed by differential scanning calorimetry (DSC) and laser desorption mass spectrometry. Purification was continued until no changes in the temperatures and widths at half-height of the main transitions were observed by DSC and no peaks due to impurities were detected by mass spectrometry. The conformational purity of sphingomyelins was confirmed by ^{1}H NMR as described by Bruzik (1988). 1,2-Dimyristoyl-*sn*-glycero-3-phosphocholine (DMPC) and *N*-(7-nitro-2-1,3-benzoxadiazol-4-yl)dilauroylphosphatidylethanolamine (DLPE-NBD) were purchased from Avanti Polar Lipids (Alabaster, AL). The purity of the lipids was confirmed by thin-layer chromatography. Chloroform solutions of the lipids were prepared and stored at −20 °C.

Fluorescence Recovery after Photobleaching. Flat multibilayers of several hundred lamellae were prepared for FRAP, as described earlier (Vaz et al., 1989; Almeida et al., 1992) but with slight modifications. About 2−3 mg of lipid, including DLPE-NBD as a probe in a mole ratio to lipid of 1:1000, was dissolved in 0.1 mL chloroform. This probe has been shown to partition exclusively into the fluid phase when solid and fluid phases coexist (Vaz et al., 1989). The solution was deposited as successive microdrops on a siliconized microscope slide at 70 °C. Very rapid solvent evaporation formed a lipid film of about 1 cm^2. The slide was placed under vacuum for about 4 h at room temperature. The dried sample was then hydrated by placing it in a covered Petri dish containing water-soaked filter paper for 4 h at 70 °C. Excess water conditions were obtained by spreading 75 μL of pH 7.6 Hepes buffer (the same buffer used for DSC) on the lipid film and covering it with a coverslip. The edges of the coverslip were sealed with a silicone paste (S/P stopcock grease) to prevent water evaporation. The sealed lipid samples consisting of a multibilayer stack were then placed in the dark at room temperature for 2−15 days before measurements were made. Occasionally, samples were stored under the above conditions for 2−3 months and again examined. Prolonged storage produced no observable changes in the parameters determined from the FRAP measurements.

FRAP measurements were made using the Meridian Instruments (Okemos, MI) ACAS 470 interactive laser fluorescence microscope equipped with an acousto-optic modulator that rapidly changes the intensity and duration of the laser spot for sequential exposure. A circular Gaussian beam profile with a theoretical radius of 1.3 μm was obtained using a 40 × LWD phase objective with the 488 nm line from a coherent argon ion laser. The laser output was 200 mW; 95−99% of the output was used as the bleaching beam

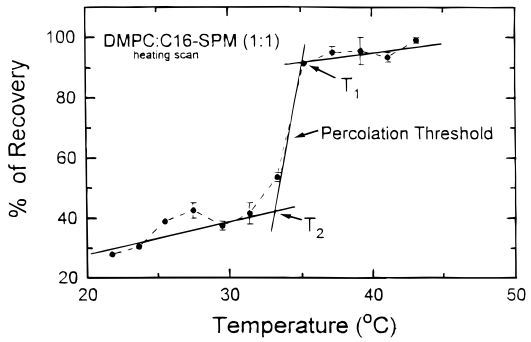

FIGURE 1: Percolation threshold is defined as the midpoint between T_1 and T_2 from the percent of recovery curves.

(blast strength) for 100−150 ms (blast time). Fluorescence recovery was monitored with the beam attenuated to 10% of the output (scan strength). Twenty time points were taken every second at earlier times (post 1). A second set of 5−7 time points at 20 s intervals was taken at later times (post 2). Fluorescence recovery was thus monitored for a total period of 120−160 s, as appropriate. The data were analyzed using the standard subroutine algorithm to give the diffusion coefficient (in centimeters squared per second) and the percent of recovery. When the modulator crystal was not energized during the delay between the monitoring scans, it was found that the scattered light that reached the sample was intense enough to cause some photobleaching. To overcome this problem, a shutter was installed in the beam path between the modulator and the sample stage. This shutter, connected to an electronic driver set up with a closed time of 19 s and an open time of 1 s, was activated after the post 1 points were collected. This cycle was repeated continuously until all the post 2 points were collected.

The temperature of the sample was controlled to ±1 °C by a Peltier KT stage controller Model 5000 (20/20 Technology, Inc., Whitehouse, NJ) built into the microscope stage. The temperature controller was calibrated using a Digi-Sense thermocouple thermometer Model No. 8528-20 (Cole-Parmer, Niles, IL). Cooling scans, initiated at a temperature well above T_c for the composition examined, were obtained by changing the temperature in 2 °C steps and holding for an equilibration period at each step of at least 30 min before each measurement. Three different regions of the slide were examined at each temperature. Heating scans were begun at 15 °C, and the same equilibration procedure was used as in the cooling curves. After a temperature-dependent recovery profile was obtained, the percolation threshold was defined as the midpoint between T_1 and T_2, as illustrated in Figure 1.

Differential Scanning Calorimetry. Dispersions of multilamellar vesicles (MLV) in excess water were prepared by mixing the components together in chloroform and evaporating the solvent in a rotary evaporator at 35 °C. Excess solvent was removed by vacuum-drying the sample at room temperature for 2−4 h. Under such conditions, the level of residual chloroform in the MLV, as tested by proton NMR (Amselem et al., 1992), is below 50 ppb. The lipid or lipid mixtures were then hydrated at 80 °C with 10 mM Hepes buffer (pH 7.6) containing 50 mM KCl, 1 mM EDTA, and 0.02% $NaNO_3$ to a final lipid concentration of 2 mg/mL. The dispersions were stirred for an hour at 80 °C and then cooled to room temperature at about 5 °C/h while stirring. In most cases, the MLV preparations were stored at 4 °C

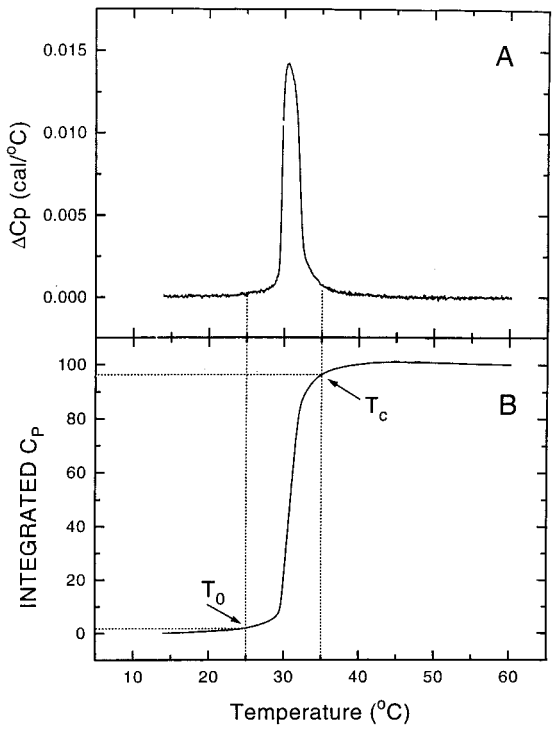

FIGURE 2: (A) Excess heat capacity vs temperature. (B) Integral of (A) showing the location of T_o, the onset temperature, and T_c, the completion temperature.

for at least 1 week before use. Heat capacity curves were obtained using a high-sensitivity Model MC-2 Microcal (Amherst, MA) differential scanning calorimeter equipped with a water circulation bath. The samples were heated from 10 to 65 °C at a rate of 20 °C/h. Four consecutive scans were made on each sample, and all of them had identical thermograms. Only the fourth heat capacity curve is shown in the Figures. To construct crude phase diagrams, the onset (T_o) and completion (T_c) temperatures of each mixture were determined from the integrated C_p vs temperature curves by arbitrarily leaving out 4% of the total heat at both sides, as illustrated in Figure 2 [for more details, see Almeida et al. (1992)].

Lipid concentrations of the fully hydrated samples were determined by organic phosphate analysis (Bartlett, 1959). Enthalpies associated with the transitions were calculated from the integrated heat capacity curves.

Chemical Stability of Phospholipids. Stability of phospholipids was tested before and after DSC runs using thin-layer chromatography as described by Barenholz and Amselem (1993). This analysis revealed that degradation products were below the detection limit of the assay (0.5%). This is in agreement with previous detailed studies on saturated phosphatidylcholine liposome stability which show a half-life at pH 7.6 of 13 months at 40 °C and 5 days at 70 °C (Grit & Crommelin, 1993). It is worth noting that sphingomyelins due to their amide bond are more chemically stable than phosphatidylcholines, which are ester phospholipids (Barenholz & Gatt, 1982).

Size Distribution Analysis. Size distribution analysis of the liposomes was determined above the gel to liquid-crystalline phase transition temperature by quasi-elastic light scattering (QUELS) at 90° using the NICOMP system equipped with NICOMP distribution analysis software (Barenholz & Amselem, 1993).

Freeze−Etch Electron Microscopy. Multilamellar vesicles of C16-SPM or C24-SPM and mixtures of these sphingomyelins with DMPC, examined by freeze−etch electron microscopy, were prepared by spraying a chloroform solution of the mixed lipids onto a glass plate, as described earlier (Thompson et al., 1985). This procedure is a convenient way to avoid possible demixing of the two lipids during solvent removal. The dried lipids were resuspended at 60 °C in the Hepes buffer to a final lipid concentration of 5 mM. The samples were then stored at 4 °C for 1 week. Small aliquots at 23 °C of the liposome preparations were ultra-fast-frozen using a Heuser-type cryopress (Med-Vac Inc., St. Louis, MO) where the aliquots were layered onto 3 mm^2 pieces of fixed rabbit lung and slammed with a gravity fall onto a liquid-helium-cooled mirror-finish copper block (Heuser, 1983). The specimens were freeze-fractured in a Balzers AF-300 freeze−etching apparatus (Balzers, Hudson, NH). Replicas, prepared by platinum/carbon rotary shadowing, were floated onto distilled water, cleaned in chloroform/methanol (2:1, v/v) to remove traces of lipids, picked up on 200-mesh grids, and observed in a Zeiss 902 electron microscope (Thompson et al., 1985).

RESULTS

Characteristics of the Pure Sphingomyelins. The uppermost curves in Figure 3A,B are representative calorimetric heating scans of purified C16- and C24-SPM liposome dispersions, respectively, in excess aqueous buffer. It can be seen that C16-SPM has a main endothermic transition centered at 41.05 ± 0.05 °C with a width at half-height, $\Delta T_{1/2}$, of 0.430 ± 0.05 °C and a transition enthalpy, ΔH, of 6.8 ± 0.2 kcal/mol. Another broad, small pretransition is located at 29.6 ± 0.4 °C with $\Delta H = 0.29 \pm 0.06$ kcal/mol.

Table 1: Thermal Transition Parameters

lipid composition	$T_M \pm$ SD (°C)	$\Delta T_{1/2} \pm$ SD (°C)	$\Delta H \pm$ SD (kcal/mol)	$T_M \pm$ SD (°C)	$\Delta T_{1/2} \pm$ SD (°C)	$\Delta H \pm$ SD (kcal/mol)
C16-SPM	29.6 ± 0.4	−	0.29 ± 0.06	41.05 ± 0.05	0.43 ± 0.05	6.8 ± 0.2
C24-SPM	39.3 ± 0.5	3.9 ± 0.9	−	45.90 ± 0.05	−	4.5 ± 0.2[b]
DMPC	−	−	−	23.91 ± 0.05	0.21 ± 0.04	10.1 ± 0.4
DMPC/C16-SPM (1:3)	−	−	−	36.84 ± 0.11	2.54 ± 0.04	13.5 ± 0.8
DMPC/C16-SPM (1:1)	−	−	−	30.58 ± 0.08	2.41 ± 0.05	16.8 ± 0.9
DMPC/C16-SPM (3:1)	−	−	−	27.46 ± 0.07	2.20 ± 0.04	16.3 ± 1.0
DMPC/C24-SPM (1:3)	−	−	−	40.09 ± 0.64	10.18 ± 2.63	10.4 ± 1.1[b]
DMPC/C24-SPM (1:1)	23.9	−	−	32.74 ± 0.69	13.53 ± 0.75	4.26 ± 0.7[b]
DMPC/C24-SPM (3:1)	23.73 ± 0.5	−	−	23.68 ± 0.06	8.23 ± 0.19	14.5 ± 0.7[b]

[a] The temperatures, T_M, refer to the maximum in the excess C_p vs T curves; $\Delta T_{1/2}$ is the width of each peak at half-height; and ΔH is the enthalpy associated with each transition shown in Figure 3. SD is the standard deviation of the measurement. [b] Total enthalpy is low because the heat capacity function is very broad (Figure 3B).

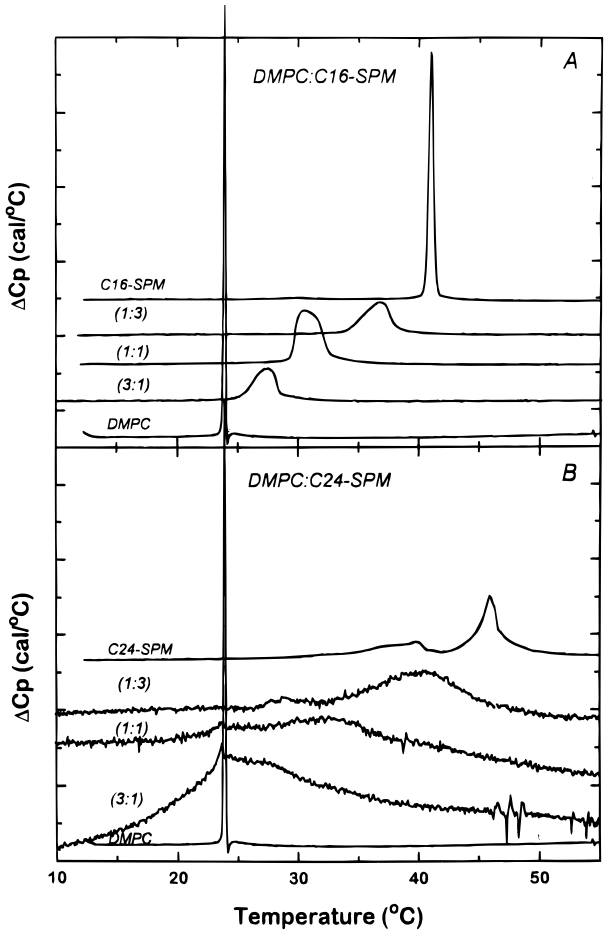

FIGURE 3: Typical excess heat capacity vs temperature curves. (A) DMPC/C16-SPM mixtures and pure components. (B) DMPC/C24-SPM mixtures and pure components.

The heating scan for the C24-SPM dispersion shows two maxima in the excess heat capacity, a minor one located at 39.3 ± 0.05 °C and a major one at 45.9 ± 0.05 °C. The total enthalpy for both endotherms calculated from the scan is 7.2 ± 0.2 kcal/mol. The temperature maxima and the enthalpies for both synthetic sphingomyelins remained unchanged upon subsequent cooling and immediate reheating. These thermal parameters are listed on Table 1. No subtransition (T_s; Biltonen & Lichtenberg, 1993) was observed for both SPMs even after 2 weeks storage at 4 °C.

Dispersions of C16-SPM and C24-SPM were examined by freeze−etch electron microscopy at 23 °C after storing for a week at 4 °C. At 23 °C, both sphingomyelins were in the gel phase. The C16-SPM dispersion consisted of typical multilamellar liposomes with a very wide range of sizes. All lipid appeared to be in the $L_{\beta'}$ gel phase (data not shown). The situation with the C24-SPM was more complex. In addition to large liposome-like structures, there were also many small unilamellar particles with diameter less than about 75 nm, as determined by QUELS. The large particles gave the appearance of an interdigitated phase (Hui et al., 1984). Representative electron micrographs are shown in Figure 4a,b. Centrifugation of the C24-SPM dispersions at 2000*g* for 10 min gave a pellet and a supernatant. Differential scanning calorimetry carried out on the resuspended pellet showed a considerable enhancement of the excess heat capacity of endotherm having lower T_m, whereas this peak was much reduced in a scan of the supernatant (data not shown). The characteristics of the particles in pellet and supernatant are given in column 1 of Table 3. It thus appears that C24-SPM forms two types of structures in the dispersion; the larger of these apparently gives rise to the excess heat capacity maximum at lower temperature, and the smaller particles generate the maximum at higher temperature. The integrated area fractions under these peaks for C24-SPM dispersions before centrifugation were 0.38 and 0.62, respectively. As noted under Materials and Methods, no chemical or stereochemical impurities were detectable in either the C16- or the C24-SPM preparation before or after the measurements.

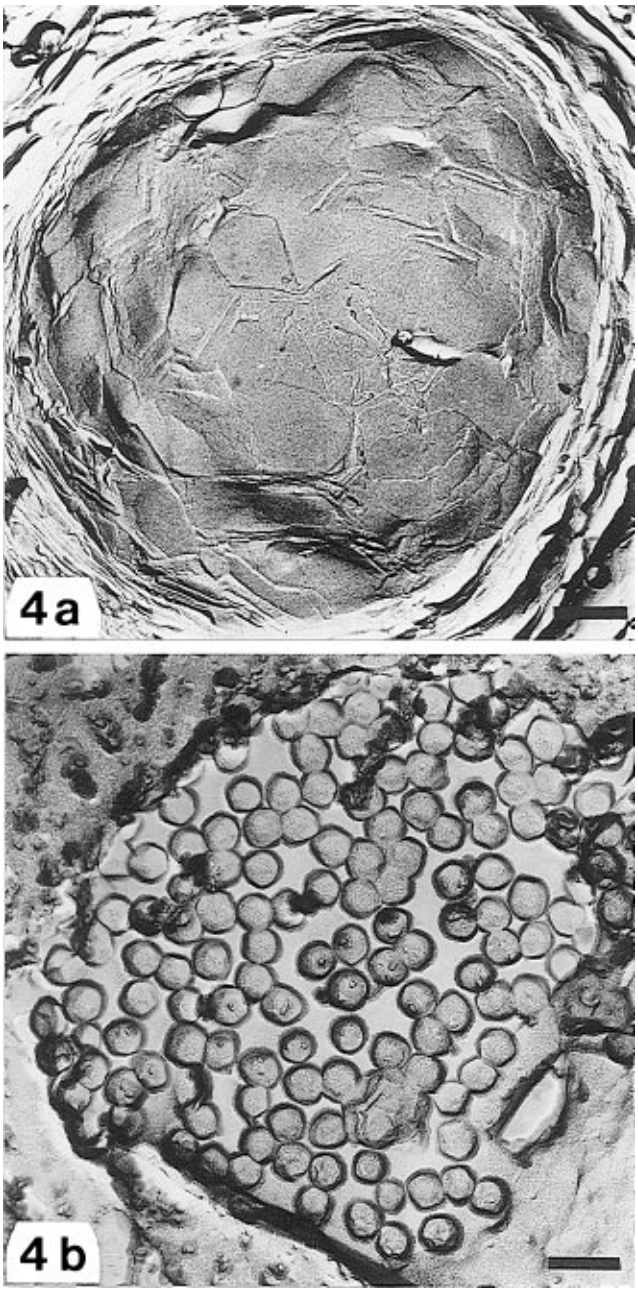

FIGURE 4: Freeze−etch electron micrographs of C24-SPM dispersions at 23 °C. (a) Large particles. (b) Small particles. The scale bar in panel a, 290 nm; panel b, 118 nm.

FRAP Studies on DMPC/SPM Bilayers. Flat multilayers consisting of several hundred bilayers of mixed lipids in excess buffer, sandwiched tightly between two glass plates, were studied by FRAP. Examinations of the multilayers by polarized light microscopy gave the typical appearance of

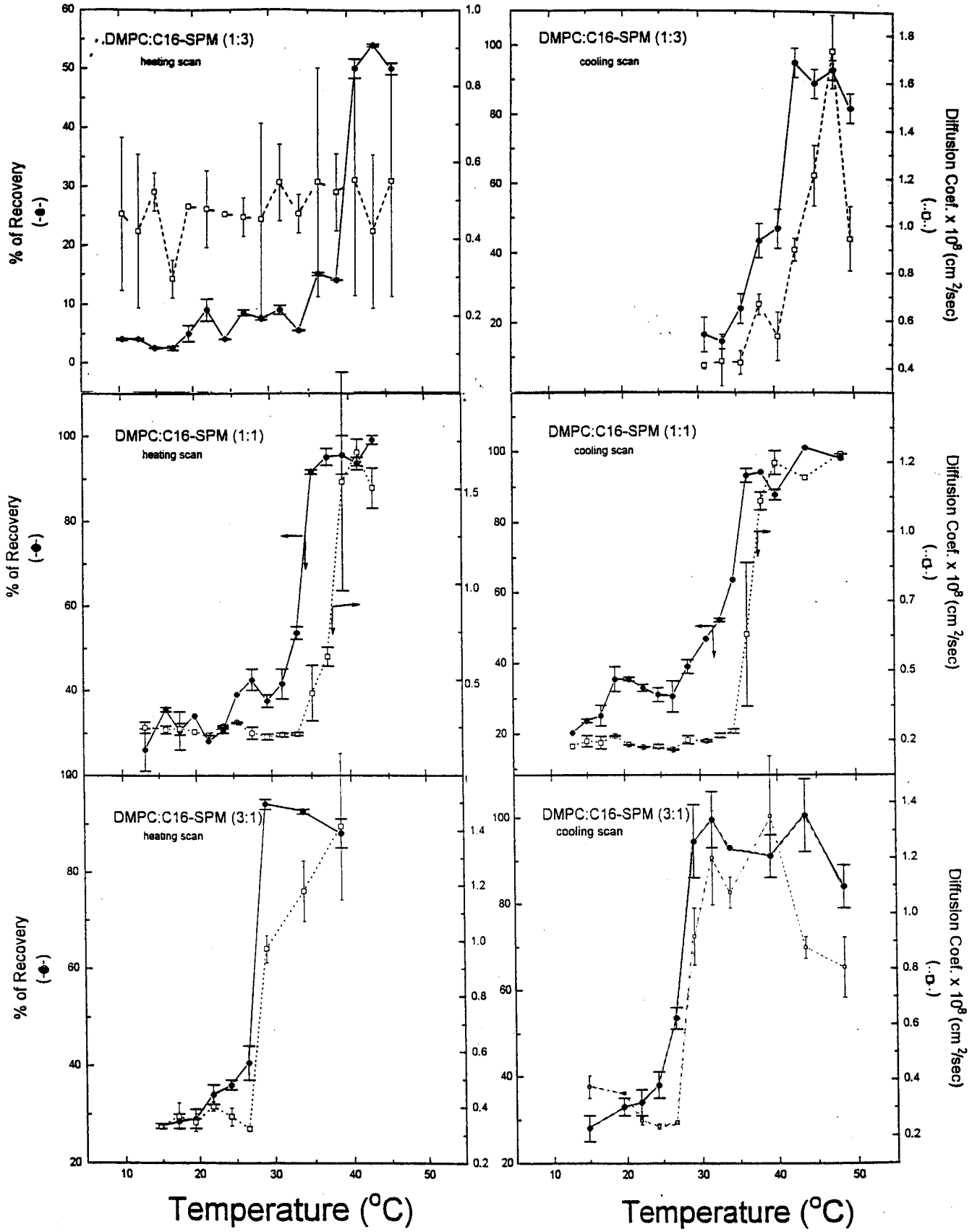

FIGURE 5: Diffusion (open squares) and percent of recovery (filled circles) as a function of temperature from heating (left side) and cooling (right side) scans in DMPC/C16-SPM systems at 25:75 (top), 50:50 (middle), and 75:25 (bottom) mole ratios. Each point represents an average of three measurements in the same sample, and the error bars are the corresponding standard deviations.

multilamellar systems. No breakup or disorganization of this structure was visible either before or after the experiment, or after prolonged storage.

Figures 5 and 6 show the diffusion coefficient (open squares) and the percent recovery of fluorescence after photobleaching (filled circles) as a function of the temper-

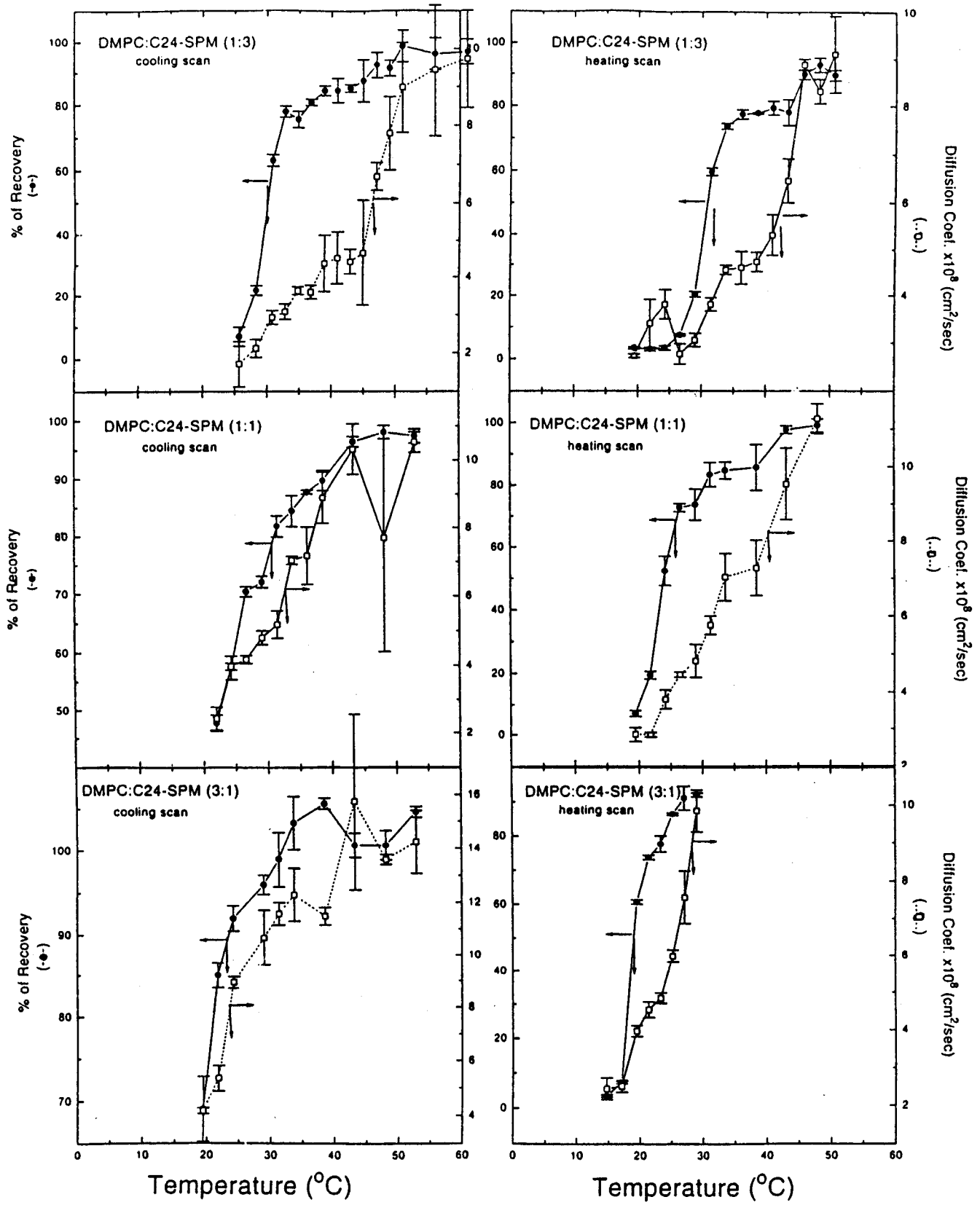

FIGURE 6: Diffusion (open squares) and percent of recovery (filled circles) as a function of temperature from heating (left side) and cooling (right side) scans in DMPC/C24-SPM systems at 25:75 (top), 50:50 (middle), and 75:25 (bottom) mole ratios. Each point represents an average of three measurements in the same sample, and the error bars are the corresponding standard deviations.

ature for DMPC/C16-SPM and DMPC/C24-SPM systems. Paired heating and cooling scans are on the left and right sides, respectively, of these figures. In general, when the bilayers were all fluid the recoveries were close to 100%, and the diffusion coefficients were greater than 1.0×10^{-8} $cm^2\ s^{-1}$. As the temperatures of the systems were lowered to bring them into the two-phase coexistence region, both the percent recovery and diffusion coefficients decreased rapidly. In all mixtures, the abrupt decrease in the percent recovery occurred at a lower temperature than did the change

Table 2: Percolation Thresholds

% of C16-SPM	T_o[a] (°C)	percolation threshold (heating)	percolation threshold (cooling)	T_c[a] (°C)
25	25	27.7	27.7	28.5
50	29.2	33.75	33.75	35.5
75	34.1	39.2	39.2	39.2
% of C24-SPM	T_o (°C)	percolation threshold (heating)	percolation threshold (cooling)	T_c[a] (°C)
25	17.17	19.5	23.5	42.17
50	20.65	22.8	26.3	43
75	27	29.18	30	48.26

[a] T_o is the onset and T_c the completion temperatures as shown in Figure 2.

in diffusion coefficient. The percolation thresholds derived from the recovery data, as illustrated in Figure 1, are listed in Table 2. Present also in the diffusion data was a very slow process accounting for 65−95% of the recovery when the systems were all gel. As the temperature range of the two-phase region was entered, the fast diffusion process rapidly became dominant. In contrast, DMPC/C24-SPM systems showed no fast component to lateral diffusion when the bilayers were all gel. Any slow diffusion component was too slow to determine, and the measured diffusion coefficient was operationally zero. In these systems, fast diffusion appeared first at the percolation threshold.

Characteristics of DMPC/SPM Dispersions. In order to establish rough phase diagrams for dispersions of the mixed lipids, differential scanning calorimetry studies were carried out. Representative thermograms of fully hydrated DMPC/C16-SPM mixtures, all previously annealed in the liquid-crystalline state and then stored at 4 °C, are shown in Figure 3A. As is the case for the pure components, upon heating, a single, broadened endothermic transition can be seen for each mixture. As the mole fraction of DMPC increased, the transition shifted progressively to lower temperatures. The thermal parameters for these systems are given in Table 1.

The situation is more complex for DMPC/C24-SPM mixtures, as can be seen in Figure 3B. In the three mixtures examined, two maxima are visible in the excess heat capacity vs temperature functions, which are reminiscent of the behavior of the pure C24-SPM representing the large and small particles observed in the electron micrographs. However, the temperatures of these maxima decrease and broaden progressively with increasing DMPC fraction. In the 1:1 and 3:1 (DMPC/C24-SPM) mixtures, a maximum very close to that of pure DMPC is also discernible. This feature was reproducible and also did not disappear on successive scans. It therefore is unlikely to be due to incomplete mixing of the components. No peaks corresponding to pure C24-SPM are visible in any of the scans of the mixtures.

Freeze−etch electron microscopy carried out at 23 °C on annealed mixtures of DMPC/C16-SPM showed multilamellar liposomes of many sizes. All lipid appeared in the rippled $P_{\beta'}$ gel phase (data not shown). A similar study carried out on DMPC/C24-SPM mixtures showed that at 23 °C the dispersions consisted of large multilamellar vesicles and smaller structures 40−75 nm in diameter. The proportion of multilamellar vesicles seemed to be the greatest in 3:1 DMPC/C24-SPM mixtures. The small structures in many electron micrographs appeared to be in the act of forming

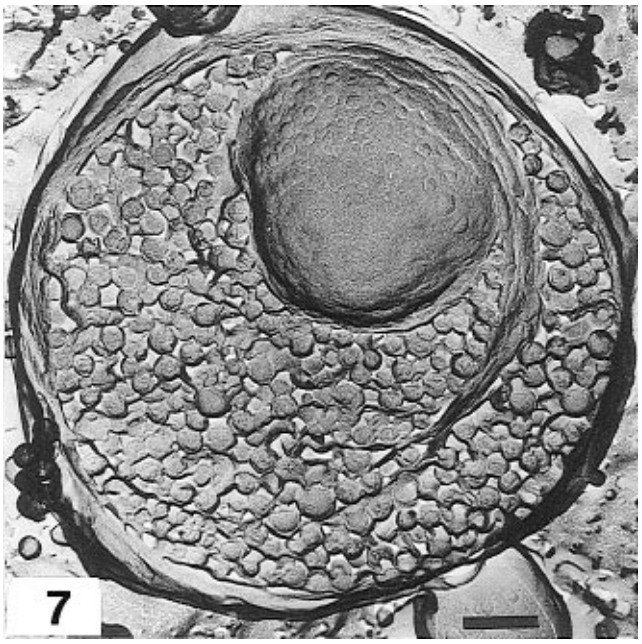

FIGURE 7: Freeze−etch electron micrograph of a C24-SPM/DMPC (1:1) mixture in aqueous dispersion at 23 °C. The scale bar is 196 nm.

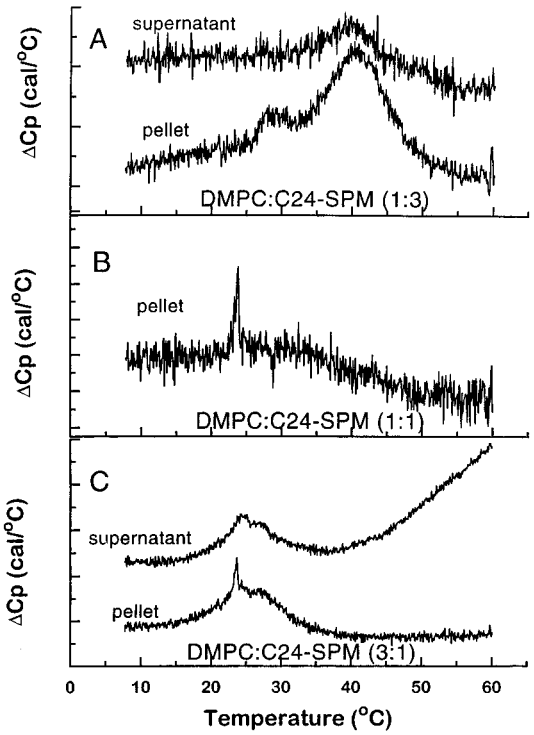

FIGURE 8: Excess heat capacity vs temperature scans for C24-SPM/DMPC dispersions, pellets, and supernatants. (A) 3:1. (B) 1:1. (C) 1:3.

from multilamellar structures in which whole lamellae seemed to be fragmenting. This is shown in Figure 7. The fraction of small objects increased with storage time at 4 °C. Each of the three mixtures was separated by centrifugation into pellet and supernatant fractions. DSC scans on the DMPC/C24-SPM 1:3 fractions were very similar to the original dispersion shown in Figure 8A. However, for the 1:1 and 3:1 mixtures, the pellets had a sharp peak at the transition temperature of DMPC (23.9 °C). This peak was absent from the supernatant fractions (Figure 8B,C). Freeze−fracture electron microscopy also showed the presence of

Table 3: Particle Sizes for C24-SPM/DMPC Mixtures

	total system composition C24-SPM/DMPC							
	1/0		1/3		1/1		3/1	
	pellet	supernatant	pellet	supernatant	pellet	supernatant	pellet	supernatant
final composition	1/0	1/0	1/3	1/3	1/1	1/1	2/1	4/1
excess heat capacity maxima (°C)	40.24 46.28	36.3 46.1	23.5 26.8	24.75	23.9[c]	24.1 32.0	24.1 39.2	40.2
diameter: QUELS[a] (nm−%)	12.6−1 118−15 752−84	60−42 249−58	48−9.55 245−90.5	81−32 296−68	104−13 356−87	62−39 192−61	59−11 247−88	67−40 239−60
diameter: electron microscopy[b] (nm)	ND	62−78 140−170	ND	91−115 400−780	ND	60−140 1200	ND	ND

[a] All QUELS measurements were made at 55 °C where all systems were fluid. Percent refers to percent of system with that mean diameter. [b] The freeze−fracture micrographs were done at 23 °C and on the pellets only. [c] There are two additional very small transitions at 36.3 and 39.3 °C.

multilamellar liposomes in the $P_{\beta'}$ phase in these pellets. From DSC data, it also appears that the fraction of the large objects contains mixtures of the two lipids in coexistence with immiscible DMPC (Figure 8). Smaller structures containing both DMPC and C24-SPM were also present. It is not clear if the immiscible DMPC is present as macroscopically separate particles or as a separate phase in the same MLV. The characteristics of the original dispersions, pellets, and supernatants of the three DMPC/C24-SPM mixtures are compared in columns 2, 3, and 4 of Table 3.

DISCUSSION

The two synthetic sphingomyelins used in this study have two endothermic transitions that are reversible and highly reproducible upon cooling and immediate reheating. The low-temperature transition in C16-SPM clearly resembles a pretransition and probably is similar to those observed in nearly symmetric disaturated phosphatidylcholine dispersions (Lin et al., 1991; Biltonen & Lichtenberg, 1993); no subtransition was observed even after 2 weeks storage at 4 °C. Below the pretransition, the acyl chains of C16-SPM are tilted with respect to the bilayer normal, and these acyl chains are packed laterally in the $L_{\beta'}$ phase. Upon heating, a transition to the $P_{\beta'}$ phase occurs in which the lipid molecule as a whole undergoes rotational motion around its long molecular axis but most of the acyl chains are still in the *all-trans* configuration and tilted with respect to the bilayer normal. This $P_{\beta'}$ phase has a characteristic wave-like surface pattern, a periodic ripple. The high-temperature endotherm is the main transition temperature of the bilayer, in which the lower segments of the acyl chains undergo rapid *trans*−*gauche* isomerizations about the C−C bonds to give the liquid-crystalline L_α phase. In this phase, the acyl chains are roughly perpendicular to the bilayer surface and are packed in a one-dimensional, disordered hexagonal lattice. Our freeze−fracture electron microscopy data on D-*erythro*-C16-SPM (data not shown) are very similar to previous data obtained for D,L-*erythro*-C16-SPM [figure 6 of Lentz et al. (1981)]. Support for this phase structure is based on X-ray diffraction (Calhoun & Shipley, 1979) and DSC studies on semisynthetic C16-SPM (Calhoun & Shipley, 1979; Cohen et al., 1984). Fully synthetic D,L-*erythro* racemic mixtures also show a similar thermotropic behavior (Barenholz et al., 1976). The $P_{\beta'}$ phase was previously seen in bovine brain sphingomyelin in freeze−fracture electron micrographs (Hui et al., 1980).

The phase behavior observed for C24-SPM conforms to the prediction based on the value of the normalized chain-length asymmetry parameter ($\Delta C/CL$) as defined by Huang and Mason (1986). They calculate that for C24-SPM, the value of $\Delta C/CL$ is 0.46 (compared with a $\Delta C/CL$ of 0.17 for C16-SPM), which suggests that the phase behavior of this sphingomyelin will be very different from that of C16-SPM. It is expected that in excess water, below the main transition temperature, these very asymmetric lipid molecules tend to form a mixed interdigitated bilayer. This packing motif is characterized by the longer acyl chain extending completely across the whole width of the hydrocarbon core of the bilayer, whereas the two shorter acyl chains, each one from the lipid in the opposing leaflets, meet end-to-end in the bilayer midplane. The structure of the phase present at temperatures between the two endotherms could be a rippled lamellar ($P_{\beta'}$), partially interdigitated gel phase, as has been shown in D,L-*erythro*-C24-SPM (Levin et al., 1985) and in the semisynthetic C24-SPM (McIntosh et al., 1992). In this gel phase, the saturated 24-carbon acyl chains in one monolayer cross the bilayer center and oppose the shorter sphingosine chains from the other monolayer. The high-temperature endotherm (upon heating) is the main transition temperature which represents the transition to the L_α liquid-crystalline phase. Recently, Lewis et al. (1994) showed that a large group of phosphatidylcholines (PCs) all having chain mismatch demonstrate a behavior of mixed interdigitated gel phase. These hydrated PCs showed unique thermotropic behavior of two exotherms upon cooling. Due to technical limitations, no cooling scan was performed for C24-SPM; thus, it is difficult to compare it to the PCs studied by Lewis et al. (1994).

As a result of the differences in the calorimetric scans of the two pure sphingomyelins, it is not surprising to find differences in the DSC scans of each sphingomyelin mixed with the symmetric, fully saturated phosphatidylcholine, DMPC. The three DMPC/C16-SPM mixtures studied exhibited a linear composition dependence of the main transition temperature, suggesting nearly ideal miscibility of the two types of molecules. The main transition was also not dependent on the thermal history of the sample and remained completely reversible upon subsequent heatings and coolings, which also strongly suggests good miscibility of the components.

The phase diagram for DMPC/C16-SPM is shown in Figure 9A. It is somewhat similar to the diagram obtained for a racemic mixture of D,L-*erythro*-C16-SPM/DMPC using diphenylhexatriene fluorescence anisotropy measurements (Lentz et al., 1981). The percolation thresholds, shown as filled triangles, lie close to the liquidus. This situation is

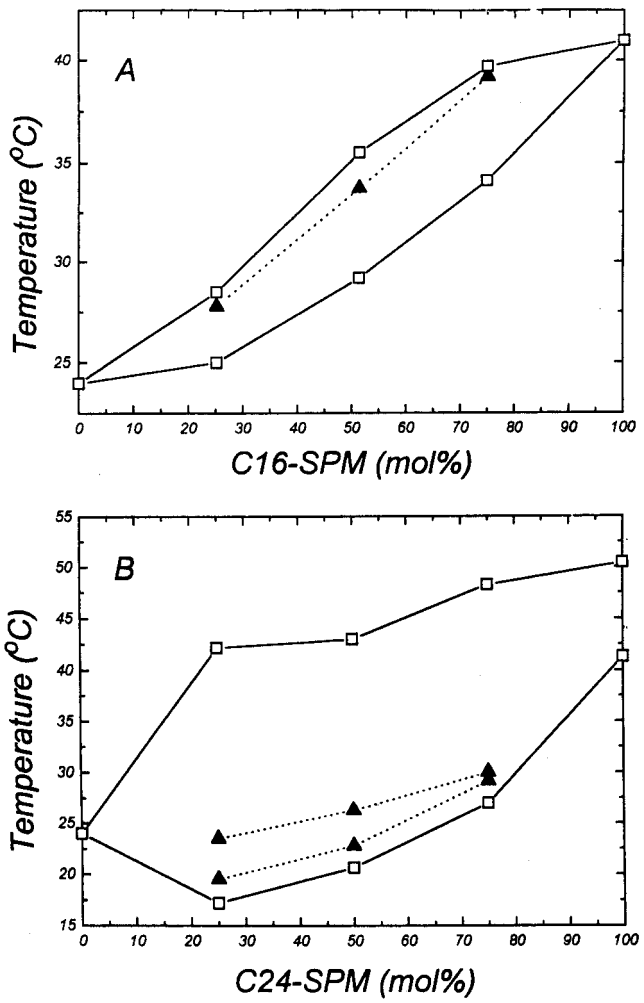

FIGURE 9: Differential scanning calorimetry based phase diagrams for (A) C16-SPM/DMPC and (B) C24-SPM/DMPC. The open squares are onset and completion temperatures. The filled triangles are the FRAP-derived percolation thresholds. In (B), the heating and cooling scans give slightly different percolation loci. The reader should be aware of the differences between DSC (aqueous dispersions) and FRAP (flat multibilayers) for the C24-SPM/DMPC system (see Discussion).

very similar to that found for the peritectic system DMPC/distearoylphosphatidylcholine mixture and indicates that the gel phase has a reticular or dendritic structure (Vaz et al., 1989).

Analysis of the DMPC/C24-SPM data is much more difficult. The DSC and size distribution (Table 3) and electron microscopy (Figure 4) data clearly show that the aqueous dispersion includes two types of assemblies differing in size. Fractions enriched with either large or small particles were obtained by differential centrifugation (Table 3). The supernatant is enriched with smaller particles. The ability to interdigitate and especially the coexistence of domains of each of the two forms of interdigitating molecules in a continuum of noninterdigitating molecules may be the driving force for the formation (budding, fission, and/or fragmentation) of smaller particles (nonspherical vesicles and/or flat bilayers; Figures 4b and 7, and Table 3) from the larger ones upon cooling. This is in agreement with the budding and fission which was observed for bovine brain SPM and was attributed to the coexistence of SPM molecules which favor higher curvature regions with those that prefer lower curvature (Dobereiner et al., 1993). This is supported by the fact that the smaller particles have a higher T_m than the larger vesicles (mostly MLV), which is usually not the case for symmetric disaturated PCs (Biltonen & Lichtenberg, 1993). In the mixtures of DMPC/C24-SPM, these two types of structures are also visible (Figure 7). Recently, Mason et al. (1995), using DSC and negative-staining electron microscopy, demonstrated a similar lamellar phase polymorphism for PCs having acyl chain mismatch. These authors relate the above polymorphism to the packing parameter [as defined by Israelachvili (1991)]. Asymmetric PCs have a wedge-like shape, with a smaller packing parameter than symmetric PCs having identical numbers of carbon atoms. This wedge shape is the reason for interdigitation, or for formation of particles having highly curved regions. Therefore, the flat regions (or vesicles) will consist mainly of interdigitated molecules, while the curved domains (or vesicles) will be enriched with noninterdigitating lipid molecules. A similar explanation may be applied to asymmetric SPM species. C24-SPM, with its one long chain and a second short methylene chain, is wedge-shaped in longitudinal cross section. Thus, two basic packing geometries are possible. One geometry is of interdigitated bilayers, of which there are two forms (Levin et al., 1985). These two forms can exist either in vesicles (MLV, or flat, smaller vesicles) or in a flat disk-like organization. The other geometry is of noninterdigitated bilayers in spheres, cylinders, or regions of high curvature. It was much easier to observe by electron microscopy interdigitating gel phase domains in MLV than in the smaller particles in C24-SPM dispersions (data not shown). The dispersions composed of mixtures of DMPC/C24-SPM show similar behavior to C24-SPM; however, the two characteristic transitions decrease in temperature with increasing DMPC content, and, in addition, in the two mixtures with the higher DMPC content, a peak suggesting the presence of pure DMPC phase appears in the pellet enriched with the larger particles (Figure 8B,C). In these preparations, typical MLV are also seen. It thus appears that the two forms of C24-SPM seen in dispersions can accommodate DMPC up to a point, and in so doing their transition temperatures decrease proportionally.

As the fraction of smaller particles increases upon storage time at 4 °C, it can be assumed that at high temperatures in the all-fluid state, C24-SPM and its mixtures with DMPC are present mainly as multilamellar structures. When the temperature is lowered, the electron micrographs indicate that gel interdigitated domains rich in C24-SPM are formed. These domains, which have the packing geometry of the higher-melting smaller particles, grow to large size in a continuous phase of fluid bilayer. In dispersions, these gel structures at some point break away from the MLV to form the smaller particles, while the remainder forms the larger structures seen in the electron micrographs. This mechanism is supported by the difference in lipid composition of the pellet and supernatant resulting from centrifuging a dispersion of C24-SPM/DMPC of 3:1 mole ratio, the pellet having a mole ratio of C24-SPM/DMPC lower than that of the supernatant (2:1 and 4:1, respectively; see last two columns in Table 3).

What, then, is the relevance of the DSC and EM data obtained in aqueous dispersions to the conditions that obtain in the FRAP experiment in the hydrated multibilayers sandwiched between two glass plates? It seems that the flat multibilayers used for the FRAP experiments and the aqueous

dispersions are not identical due to restrictions imposed on the former. However, there was no visible breakup of these multibilayers evident by polarized light microscopy at any temperature (15−60 °C), or even after 2 months storage at 20 °C. This suggests that the initial solid domains in the multibilayers examined by FRAP remain in the macroscopically stable lamellar structure in which they formed. That is, in the FRAP experiments, the lamellae remain flat, and there is no breakup into the two classes of particles. Therefore, we do not expect two main transitions related to lamellar phase polymorphism, and the thermotropic behavior of the larger (less curved) particles may be more relevant to the construction of the phase diagram. In the multilayers of the FRAP experiments, these large solid domains divide the fluid phase into a reticular continuum that is not disconnected until the system is nearly all-solid. This behavior is similar to that found for the eutectic system composed of di-C17-PC and C22C12-PC at high C22C12-PC mole fractions (Bultman et al., 1991).

This study shows clearly that the mixing of DMPC with C24-SPM in bilayers either of the various assemblies present in the aqueous dispersions or of the multibilayers used in the FRAP experiments is very nonideal. It is also apparent that the nonideality must be primarily due to the intramolecular methylene chain mismatch in this sphingomyelin and the intermolecular methylene chain mismatch with DMPC. Since this sort of chain mismatch exists in plasma membranes of mammalian cells, the mixing of natural sphingomyelin with the other, mostly unsaturated and close to symmetric, lipid components of these membranes must also be highly nonideal. Therefore, the presence of sphingomyelins having chain mismatch in biological membranes (Barenholz, 1984) presents a condition necessary for phase domain formation as was observed for MLV composed of egg PC and bovine brain SPM which is enriched with long acyl chain SPM (Barenholz, 1984), or in plasma membranes of rat cardiomyocytes (Yechiel et al., 1985). Such a composition is a good example of the ability to couple phase separation and curvature, which may explain the cell shapes and shape transitions (Sackman, 1994).

Although, as discussed above, it seems that in many aspects asymmetric sphingolipids and PCs behave similarly, the fact that only the former are abundant in biological membranes may have functional significance, for example, in involvement in signal transduction via the sphingomyelin cycle (Kan & Kolesnick, 1993), as well as in the formation and/or stabilization of microdomains ("rafts") and related structures [reviewed in Futerman (1995)].

ACKNOWLEDGMENT

We thank Margaretta Allietta for performing the freeze−etch electron microscopy.

REFERENCES

Almeida, P. F. F., Vaz, W. L. C., & Thompson, T. E. (1992) *Biochemistry 31*, 7198−7210.

Amselem, S., Cohen, R., Druckmann, S., Gabizon, A., Goren, D., Abra, R. M., Huang, A., New, R., & Barenholz, Y. (1992) *J. Liposome Res. 2*, 93−123.

Barenholz, Y. (1984) in *Physiology of Membrane Fluidity* (Shinitzky, M., Ed.) Vol. 1, pp 131−173, CRC Press, Boca Raton, FL.

Barenholz, Y., & Thompson, T. E. (1980) *Biochim. Biophys. Acta 604*, 129−158.

Barenholz, Y., & Gatt, S. (1982) in *Phospholipids* (Hawthorne, J. N., & Ansell, G. B., Eds.) pp 129−177, Elsevier, Amsterdam.

Barenholz, Y., & Amselem, S. (1993) in *Liposome Technology* (Gregoriadis, G., Ed.), 2nd ed., Vol. I, pp 527−616, CRC Press, Boca Raton, FL.

Barenholz, Y., Suurkuusk, J., Mountcastle, D., Thompson, T. E., & Biltonen, R. L. (1976) *Biochemistry 15*, 2441−2447.

Bartlett, G. R. (1959) *J. Biol. Chem. 234*, 466−468.

Bergelson, L. O. K., Gawrisch, K., Ferretti, J. A., & Blumenthal, R. (1995) *Mol. Membr. Biol. 12*, 1−162.

Biltonen, R. L., & Lichtenberg, D. (1993) *Chem. Phys. Lipids 64*, 129−142.

Bruzik, K. S. (1988) *Biochim. Biophys. Acta 939*, 315−326.

Bultman, T., Vaz, W. L. C., Melo, E. C. C., Sisk, R. B., & Thompson, T. E. (1991) *Biochemistry 30*, 5573−5579.

Calhoun, W. I., & Shipley, G. G. (1979) *Biochemistry 18*, 1717−1722.

Cohen, R., Barenholz, Y., Gatt, S., & Dagan, A. (1984) *Chem. Phys. Lipids 35*, 371−384.

Döbereiner, H. G., Kas, J., Noppl, D., Sprenger, I., & Sackman, E. (1993) *Biophys. J. 65*, 1396−1403.

Futerman, A. H. (1995) *Trends Cell Biol. 15*, 337−341.

Grit, M., & Crommelin, D. J. A. (1993) *Chem. Phys. Lipids 64*, 3−18.

Heuser, J. E. (1983) *J. Mol. Biol. 169*, 155−195.

Huang, C., & Mason, J. T. (1986) *Biochim. Biophys. Acta 864*, 423−470.

Hui, S. W., Stewart, T. P., & Yeagle, P. L. (1980) *Biochim. Biophys. Acta 601*, 271−281.

Hui, S. W., Mason, J. T., & Huang, C. (1984) *Biochemistry 23*, 5570−5577.

Israelachvili, J. J. (1991) *Intermolecular and Surface Forces*, 2nd ed., Academic Press, London.

Jacobson, K., & Vaz, W. L. C. (1992) *Comments Mol. Cell. Biophys. 8*, 1−114.

Kan, C. C., & Kolesnick, R. (1993) *Trends Glycosci. Glycotechnol. 5*, 99−106.

Lentz, B. R., Hoechli, M., & Barenholz, Y. (1981) *Biochemistry 20*, 6803−6809.

Levin, I. W., Thompson, T. E., Barenholz, Y., & Huang, C. (1985) *Biochemistry 24*, 6282−6286.

Lewis, R. N., McElhaney, R. N., Osterberg, F., & Gruner, S. M. (1994) *Biophys. J. 66*, 207−216.

Lin, H. N., Wang, Z. Q., & Huang, C. (1991) *Biochim. Biophys. Acta 1067*, 17−28.

McIntosh, T. J., Simon, S. A., Needham, D., & Huang, C. (1992) *Biochemistry 31*, 2012−2020.

Sackman, E. (1994) *FEBS Lett. 346*, 3−16.

Singer, S. J., & Nicholson, G. L. (1972) *Science 175*, 720−731.

Thompson, T. E., Allietta, M. A., Brown, R. E., Johnson, M. L., & Tillack, T. W. (1985) *Biochim. Biophys. Acta 817*, 229−237.

Vaz, W. L. C. (1996) in *Handbook of Nonmedical Applications of Liposomes* (Barenholz, Y., & Lasic, D. D., Eds.), Vol. II, pp 51−60, CRC Press, Boca Raton, FL.

Vaz, W. L. C., Melo, E. C. C., & Thompson, T. E. (1989) *Biophys. J. 56*, 869−876.

Yechiel, E., Barenholz, Y., & Henis, Y. I. (1985) *J. Biol. Chem. 260*, 9132−9136.

BI9625004